PCCP

Destruction and reconstruction of UO22+ using gas-phase reactions

Journal:	*Physical Chemistry Chemical Physics*
Manuscript ID	CP-ART-04-2021-001520.R1
Article Type:	Paper
Date Submitted by the Author:	06-May-2021
Complete List of Authors:	van Stipdonk, Michael J.; Duquesne University, Chemistry and Biochemistry Perez, Evan; Duquesne University, Department of Chemistry Metzler, Luke; Duquesne University Bayer School of Natural and Environmental Sciences, Bubas, Amanda; Duquesne University, Chemistry and Biochemistry Corcovilos, Theodore A.; Duquesne University, Physics Somogyi, Arpad; The Ohio State University, Campus Chemical Instrumentation Center

ARTICLE

Destruction and reconstruction of UO_2^{2+} using gas-phase reactions

Michael J. Van Stipdonk*[a], Evan H. Perez†[a], Luke J. Metzler[a], Amanda R. Bubas‡[a], Theodore Corcovilos*[b] and Arpad Somogyi[c]

Received 00th January 20xx,
Accepted 00th January 20xx

DOI: 10.1039/x0xx00000x

While the strong axial U=O bonds confer high stability and inertness to UO_2^{2+}, it has been shown that the axial oxo ligands can be eliminated or replaced in the gas-phase using collision-induced dissociation (CID) reactions. We report here tandem mass spectrometry experiments initiated with a gas-phase complex that includes UO_2^{2+} coordinated by a 2,6-difluorobenzoate ligand. After decarboxylation to form a difluorophenide coordinated uranyl ion, $[UO_2(C_6F_2H_3)]^+$, CID causes elimination of CO, and then CO and C_2H_2 in sequential dissociation steps, to leave a reactive uranium fluoride ion, $[UF_2(C_2H)]^+$. Reaction of $[UF_2(C_2H)]^+$ with CH_3OH creates $[UF_2(OCH_3)]^+$, $[UF(OCH_3)_2]^+$ and $[UF(OCH_3)_2(CH_3OH)]^+$. Cleavage of C-O bonds within these species results in the elimination of methyl cation (CH_3^+). Subsequent CID steps convert $[UF(OCH_3)_2]^+$ to $[UO_2(F)]^+$ and similarly, $[U(OCH_3)_3]^+$ to $[UO_2(OCH_3)]^+$. Our experiments show removal of *both* uranyl oxo ligands in "top-down" CID reactions and replacement in "bottom-up" ion-molecule and dissociation steps.

1 Introduction

The high stability and inertness of the U=O bonds make activation and/or functionalization of UO_2^{2+} and UO_2^+ challenging.[1-6] Identification of effective methods to activate UO_2^{2+} to produce species in lower oxidation states, or to cause exchange or substitution of an oxo ligand are of great interest and importance[7-10]. Development of efficient means for exchange or substitution of the "yl" oxo ligands may lead to improved approaches for actinide separations, or the generation of new and potentially highly reactive species. Also, Cowie and coworkers[4] have noted that the chemistry of the U=O bond is of great "academic interest" given that the lack of reactivity differs from other metal-oxo species.

Gas phase experiments provide important information about intrinsic behavior, without the complicating factors associated with the presence of solvent. Recent gas-phase studies indicate that the U=O bonds of UO_2^{2+} can be activated and substituted using collision-induced dissociation (CID)[11]. For example, Gibson and coworkers demonstrated that CID of $[UO_2(N_3)Cl_2]^-$ creates $[UO(NO)Cl_2]^-$ by elimination of N_2,[11a] and that $[UO_2(NCO)Cl_2]^-$ dissociates by elimination of CO_2 to make $[UONCl_2]^-$.[11b] Our group created $[NUO]^+$ by rearrangement and fragmentation of $[UO_2(N{\equiv}C)]^+$, which was generated by homolytic C-C bond cleavage during CID of $[UO_2(N{\equiv}C\text{-}CH_3)]^{2+}$.[11c] More recent experiments in our laboratory have shown that CID of $[UO_2(O_2C\text{-}C{\equiv}CH]^+$ can be used to prepare $[UO_2(C{\equiv}CH)]^+$ by decarboxylation, and $[UO_2(C{\equiv}CH)]^+$ dissociates by elimination of CO to furnish the U-methylidyne species $[OUCH]^+$.[11f,g] Each of these gas-phase examples involves the substitution of one axial oxo ligand from the UO_2 moiety in a gas-phase reaction.

In general, the condensed-phase approaches involve some aspect of reductive functionalization and metalation, silylation, borylation or alkylation, for example, of the oxo ligands of UO_2.[4] The gas-phase oxo-elimination reactions appear to be thermochemically driven by rearrangement, formation of C-O and N-O bonds with the axial O atoms of UO_2, and the loss of small neutral molecules such as CO_2[11a], N_2[11b] and CO[11c,d,f,g]. While the link to condensed-phase reactivity can be tenuous, the importance of gas-phase reactivity data is that it identifies *intrinsic* chemistry.

In the study reported here, multidimensional (MS^n) tandem mass spectrometry experiments were used to convert a precursor ion containing $U^{VI}O_2^{2+}$ to product ions that include U that is formally in the IV or III oxidation state, which appear to be much more reactive species. What is more important is that the product ions with lower formal oxidation states lack *both* uranyl axial oxo ligands. Subsequent ion-molecule and dissociation reactions with the reduced product ions were then used to oxidize U and "reconstruct" the $U^{VI}O_2$ moiety. To the best of our knowledge, this is the first demonstration that the oxo ligands can be removed and replaced in a single gas-phase experiment.

[a] *Department of Chemistry and Biochemistry, Duquesne University, Pittsburgh, PA 15282, USA*
[b] *Department of Physics, Duquesne University, Pittsburgh, PA 15282, USA*
[c] *Campus Chemical Instrument Center, The Ohio State University, Columbus, OH 43210, USA.*
* To whom correspondence should be addressed: Duquesne University, Dept. of Chemistry and Biochemistry, 600 Forbes Ave, 308 Mellon Hall, Pittsburgh, PA 15282, USA. Email: vanstipdonkm@duq.edu and corcovilost@duq.edu
† Current address: Department of Chemistry, Yale University, New Haven, CT 06520, USA
‡ Current address: Department of Chemistry, University of Utah, Salt Lake City, UT 84112, USA
Electronic Supplementary Information (ESI) available: See DOI: 10.1039/x0xx00000x

2 Experimental Methods

2.1 Sample Preparation

Methanol (CH_3OH), labeled methanol (CD_3OH), ethanol (CH_3CH_2OH) and 2,6-difluorobenzoic acid were purchased from Millipore-Sigma (St. Louis, MO) and used as received. The sample used to prepare gas-phase $[UO_2(O_2C\text{-}C_6F_2H_3)]^+$ was created by combining 2-3 mg of $U^{VI}O_3$ (Strem Chemicals, Newburyport MA), corresponding to approximately 7×10^{-6} to 1×10^{-5} moles, with a 2-fold mole excess of difluorobenzoic acid (Sigma Aldrich, St. Louis MO) and 400 µL of deionized/distilled H_2O in a glass scintillation vial. The solutions were incubated on a hot plate at 70°C for 12 hours. *Caution: uranium oxide is radioactive (α- and γ-emitter), and proper shielding, waste disposal and personal protective gear should be used when handling the material*. When cooled, 20 µL of the resulting solution was diluted with 800 µL of 90:10 (by volume) H_2O:CH_3CH_2OH and used without further work up as the spray solution for electrospray ionization (ESI).

ESI and CID experiments were performed on a ThermoScientific (San Jose, CA) LTQ-XL linear ion trap (LIT) mass spectrometer. Solutions for ESI were infused into the instrument using the incorporated syringe pump at a flow rate of 5 µL/min. In the positive ion mode, the auto-tune routine within the LTQ Tune program was used to optimize the atmospheric pressure ionization stack settings for the instrument (lens voltages, quadrupole and octopole voltage offsets, etc.) to achieve maximum transmission of singly charged ions such as $[UO_2(O_2C\text{-}C_6F_2H_3)(CH_3CH_2OH)_2]^+$ to the LIT. Helium was used as the bath/buffer gas to improve trapping efficiency and as the collision gas for CID experiments.

For multiple-stage (MS^n) CID experiments to probe fragmentation pathways, precursor ions were isolated using a width of 1.0 to 1.5 mass to charge (*m/z*) units. The exact value was determined empirically to provide maximum ion intensity while ensuring isolation of a single isotopic peak. To probe CID behavior, the (mass) normalized collision energy (NCE, as defined by ThermoScientific) was set between 5 and 18%, which corresponds to 0.075 - 0.27 V applied for CID with the current instrument calibration. The activation Q, which defines the frequency of the applied radio frequency potential, was set at 0.30 and a 30 ms activation time was used.

The linear ion trap has been modified to allow the mixing of reagents with the helium buffer gas before introduction into the ion trap[12a,12b]. Liquid reagents are introduced into the manifold from a metered syringe pump, where they evaporate. The partial pressure of these reagents may be controlled through the syringe pump rate, the helium flow rate, and by heating or cooling the manifold, which is done by wrapping the manifold tubing with a temperature-controlled water coil. All gas ports are controlled by manually actuated precision needle valves, which provide control of the flow rates.

To probe gas-phase reactions of selected precursor ions with background neutrals, ions were isolated using widths of 1-2 *m/z* units. Here too, the specific width used was chosen empirically to ensure maximum ion isolation efficiency. The ions were then stored in the LIT for periods ranging from 1 ms to 10 s. When examining ion-molecule reactions (IMRs), our intent was not to measure or report rates or rate constants, but to identify the *pathways* by which ions react with neutrals such as H_2O or CH_3OH in the LIT. Because the experiments were performed using the multi-dimensional tandem mass spectrometry capabilities of the linear ion trap, care had to be taken to ensure that enough neutral reagent was present in the ion trap for ion-molecule reaction studies, without hampering the "synthesis" of reactive species using several CID steps in series. For both CID and IMR experiments, the mass spectra displayed were created by accumulating and averaging at least 30 isolation, dissociation, and ejection/detection steps.

Independent high-resolution/high-accuracy *m/z* measurements were performed on a ThermoScientific (San Jose, CA) LTQ-Orbitrap Elite mass spectrometer using experimental conditions and settings like those outlined above for the LTQ-XL instrument. With the Orbitrap instrument, the experiments were performed with the 120,000 resolution setting, NCE values of 8 – 16%, activation Q setting of 0.25, and a 10 ms activation time. Mass spectra were collected for 1 minute at each MS^n stage.

3 Results and Discussion

Quadrupole ion traps allow "tandem in time" CID experiments, with several collisional-activation steps in series, initiated with a given precursor ion[12c]. As outlined above, our ion trap mass spectrometer modified to allow both multiple-stage CID *and* controlled introduction of neutral reagents for investigation of ion-molecule reactions. Our use of the difluorobenzoate ligand in the present experiments was motivated by two prior observations. The first was that CID of anionic complexes with trifluoroacetic acid and superoxide ligands ultimately created $[OU(F)_4]^-$ by fluoride transfer and elimination of a single axial oxo ligand[11h]. The second was the demonstration that cationic and anionic UO_2 complexes with difluoro- and pentafluorobenzoate[11i,11j] fragment by reactions that appeared to involve elimination of the axial oxo ligands. To accompany discussion of the experiments below, a list of product ions from CID and ion-molecule reactions are provided in Table S1 of the supplemental information. Only those species most relevant to the description of the destruction and reconstruction of UO_2 (i.e., removal and addition of the axial oxo ligands) are discussed here.

3.1 Deconstruction of UO_2 using MS^n CID

Product ion spectra generated by MS^n CID of $[UO_2(O_2C\text{-}C_6F_2H_3)(CH_3CH_2OH)_2]^+$ (*m/z* 519) are shown in Figures 1a-f. The first and second CID steps (MS^2 and MS^3 stages, Figures 1a and 1b) caused elimination of 46 mass units (the Da unit is used hereafter), corresponding to the ancillary CH_3CH_2OH ligands of the precursor complex. At the MS^4 stage (Figure 1c) CID of $[UO_2(O_2C\text{-}C_6H_3F_2)]^+$ (*m/z* 427) caused the elimination of 44 Da, which was attributed to the loss of CO_2, to generate what was assumed to be the UO_2^{2+} complex with

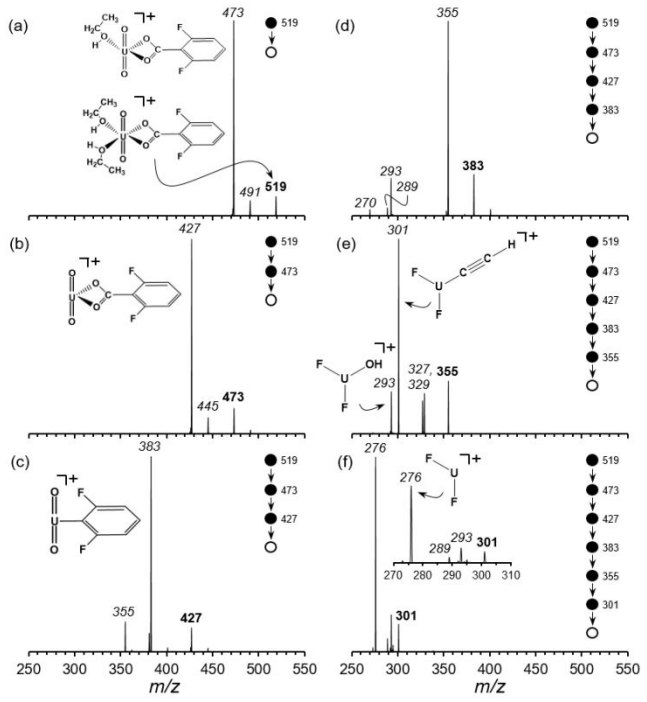

Fig. 1 Product ion spectra generated by MS^n CID of $[UO_2(O_2C\text{-}C_6F_2H_3)(CH_3CH_2OH)_2]^+$: (a) CID (MS/MS or MS^2 stage) of $[UO_2(O_2C\text{-}C_6F_2H_3)(CH_3CH_2OH)_2]^+$ (*m/z* 519), (b) CID (MS^3 stage) of $[UO_2(O_2C\text{-}C_6F_2H_3)(CH_3CH_2OH)]^+$ (*m/z* 473), (c) CID (MS^4 stage) of $[UO_2(O_2C\text{-}C_6F_2H_3)]^+$ (*m/z* 427), (d) CID (MS^5 stage) of $[UO_2(C_6F_2H_3)]^+$ (*m/z* 383), (e) CID (MS^6 stage) of *m/z* 355 and (f) CID (MS^7 stage) of *m/z* 301. The serial dissociation steps are indicated with the filled and open circles associated with each spectrum. Nominal *m/z* values are provided here. For accurate masses, see Table S1 of the supplemental information.

2,6-difluorophenide, $[UO_2(C_6H_3F_2)]^+$ (the presumed ligand shown in inset of Figure 1c). Subsequent CID of $[UO_2(C_6H_3F_2)]^+$ (*m/z* 383, MS^5 stage, Figure 1d) caused the elimination of 28 Da, assumed to be CO, to create an ion at *m/z* 355. Formation of the product ion at *m/z* 355 was surprising, because the only source of an O atom for apparent elimination of CO is the UO_2 moiety, and loss of CO thus infers activation of a U=O bond of UO_2.

In the next CID step (MS^6 stage, Figure 1e), dissociation of the ion at *m/z* 355 created product ions and *m/z* 329 and 327 by elimination of 26 Da and 28 Da, assumed to be C_2H_2 and CO, respectively, and a product ion at *m/z* 301 (assumed to involve the elimination of both C_2H_2 and CO). The ion at *m/z* 301 was also generated when the species at *m/z* 329 and *m/z* 327 were independently isolated and subjected to CID. Based on the neutral losses in the sequential dissociation reactions, the ion at nominal *m/z* 301 was assigned the composition $[UF_2(C_2H)]^+$. The combined loss of 2 CO molecules and C_2H_2, indicates decomposition of both the UO_2 moiety and difluorophenide ligand generated by decarboxylation. Subsequent CID of $[UF_2(C_2H)]^+$ (MS^7 stage, Figure 1f) caused the elimination of 25 Da (C_2H) to produce a terminal dissociation product at *m/z* 276, which was assumed to have a composition of $[UF_2]^+$.

To support ion composition assignments the MS^n CID of $[UO_2(O_2C\text{-}C_6F_2H_3)(CH_3CH_2OH)_2]^+$ was also measured using a high-resolution/mass accuracy orbitrap mass spectrometer. Comparisons of accurate *m/z* measurements to theoretical

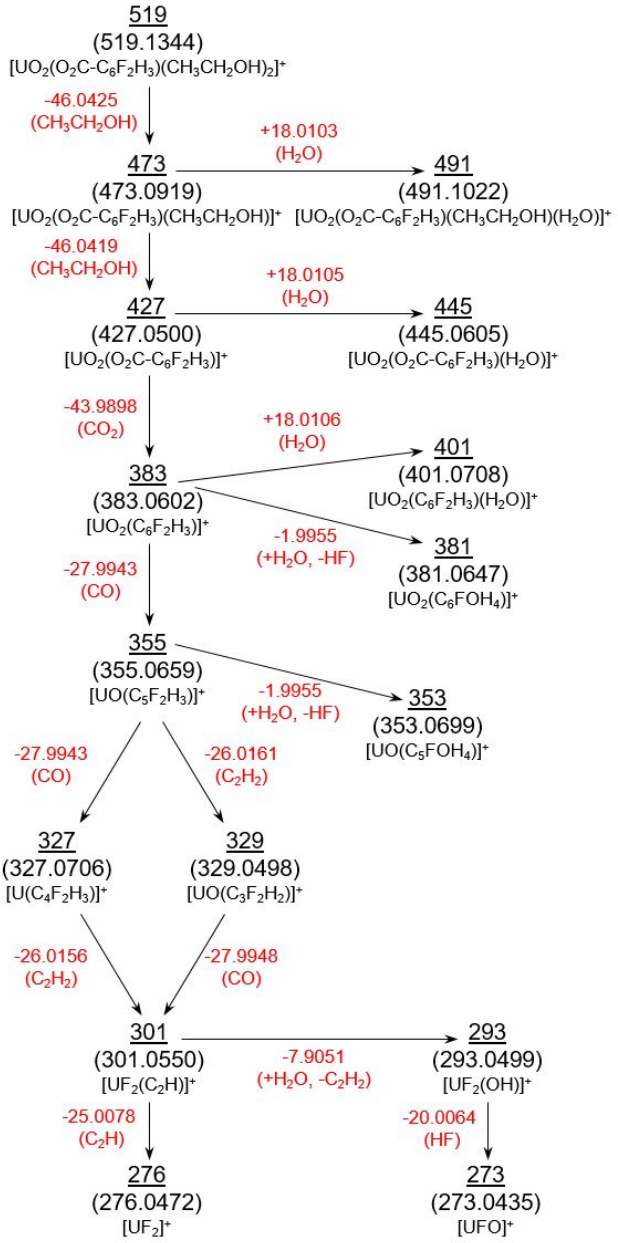

Scheme 1 Major relevant dissociation pathways for $[UO_2(O_2C\text{-}C_6F_2H_3)(CH_3CH_2OH)_2]^+$ including accurate mass values for ionic and neutral species, and proposed compositions.

monoisotopic values along with molecular formula assignments are provided in Table S2 of the supporting information. In Scheme 1, the major relevant dissociation pathways for $[UO_2(O_2C\text{-}C_6F_2H_3)(CH_3CH_2OH)_2]^+$ are summarized and labeled with accurate values for ionic and neutral species. Most important to this study, the accurate *m/z* values for the species assumed to be $[UO_2(O_2C\text{-}C_6H_3F_2)]^+$ (nominal *m/z* 427) and $[UO_2(C_6H_3F_2)]^+$ (nominal *m/z* 383) differs from the theoretical mass for the corresponding molecular formulae of $[C_7H_3F_2O_4U]$ and $[C_6H_3F_2O_2U]$ by only 0.7 mDa (~1.64 ppm error) and 0.6 mDa (~1.57 ppm error) and supports the composition assignments. The product ion at nominal *m/z* 355 created by CID of $[UO_2(C_6H_3F_2)]^+$ has a measured accurate *m/z*

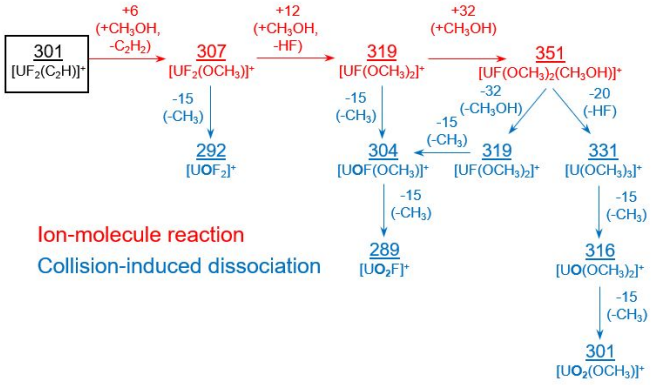

Scheme 2 Reaction pathways (dissociation and ion-molecule reaction) for species created by isolation and exposure of $[UF_2(C_2H)]^+$ to ca. 1×10^{-6} torr of CH_3OH directly admitted to the ion trap mass spectrometer.

value of 355.0655, which differs from the proposed formula $[C_5H_3F_2OU]$ by 0.4 mDa (~1.13 ppm error), and the difference in measured mass between the two product ions is 27.9943 Da, compared to the theoretical mass for CO of 27.9949 and 28.0313 for C_2H_4. Similar accurate mass measurements support the composition assignments of the ions at nominal *m/z* 329, 327, 301 and 276, and the elimination of small neutral molecules such as CO and C_2H_2, in the dissociation steps.

The MS^n CID experiments combined with accurate *m/z* measurements, clearly demonstrate the removal of both axial oxo ligands of the uranyl moiety and transfer of two fluoride ligands to U. This is achieved by decomposition of the reactive difluorophenide ligand, which facilitates loss of small neutral molecules such as CO and C_2H_2. It is noteworthy that with the reasonable assumption of formal -1 charge on the F and C_2H ligands, and the overall +1 ion charge, the formal oxidation state of U is reduced from VI in $[UO_2(C_6F_2H_3)]^+$ to IV in $[UF_2(C_2H)]^+$ and finally to the III oxidation state in the terminal $[UF_2]^+$ product ion.

3.2 Reconstruction of UO_2 using Ion-Molecule and Dissociation Reactions

The next step was to probe the reactions of $[UF_2(C_2H)]^+$ with H_2O and CH_3OH, working with the hypothesis that F and C_2H ligands would be replaced by OH and OCH_3 (with concomitant loss of HF and C_2H_2 as neutral species). The product ion spectra generated by isolation (MS^8 stage) of $[UF_2(C_2H)]^+$ for reaction with H_2O are shown in Figure S1a-c of the supplemental information. The dominant product created by reaction with H_2O was $[UF_2(OH)]^+$ (*m/z* 293), likely created by simple hydrolysis and elimination of C_2H_2 (reaction 1).

(1) $[UF_2(C_2H)]^+ + H_2O \rightarrow [UF_2(OH)]^+ + C_2H_2$

Subsequent CID of $[UF_2(OH)]^+$ (Figure S1d) caused elimination of 20 Da (attributed to loss of HF) to produce $[OUF]^+$ at *m/z* 273. Isolation of ions for reaction with H_2O present as background species in the orbitrap instrument allowed for confirmation of composition assignments of $[UF_2(OH)]^+$ and

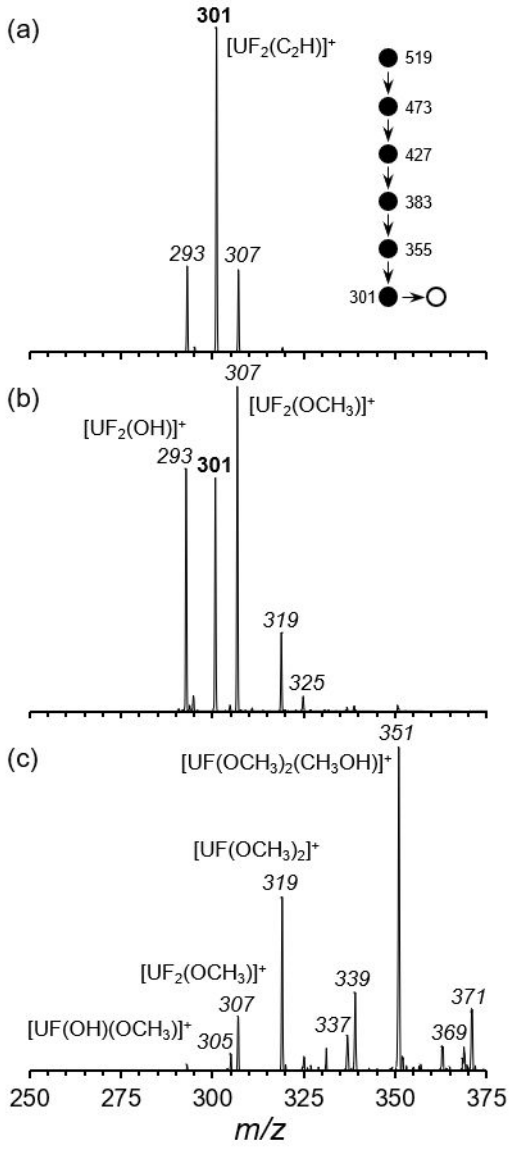

Fig. 2 Product ion spectra generated by isolation of $[UF_2(C_2H)]^+$ for reaction with CH_3OH (MS^8 stage): (a) 1 ms isolation/reaction time, (b) 10 ms isolation/reaction time and (c) 100 ms isolation time. The precursor ion is indicated by bold font. Product ions are indicated with italicized text.

$[OUF]^+$ for the species at *m/z* 293 and 273 as shown in Scheme 1.

Product ion spectra generated by reaction of $[UF_2(C_2H)]^+$ with CH_3OH (MS^8 stage) for periods ranging from 1ms to 100 ms are shown in Figures 2a-c. In this case, the data were collected using the ion trap modified for the controlled addition of neutral reagents. The general pathways identified by multiple isolation steps for reaction with ca. 1×10^{-6} torr of CH_3OH admitted directly into the ion trap and with (background) H_2O are summarized in Scheme 2.

The appearance of the product ion at *m/z* 293 ($[UF_2(OH)]^+$) in the spectra shown in Figure 2 is attributed to reaction of $[UF_2(C_2H)]^+$ with background H_2O. At relatively short isolation times (e.g. 1 and 10 ms, Figures 2a and 2b), reaction of $[UF_2(C_2H)]^+$ with CH_3OH primarily leads to an ion at *m/z* 307, which is assigned as $[UF_2(OCH_3)]^+$ generated by reaction 2. At

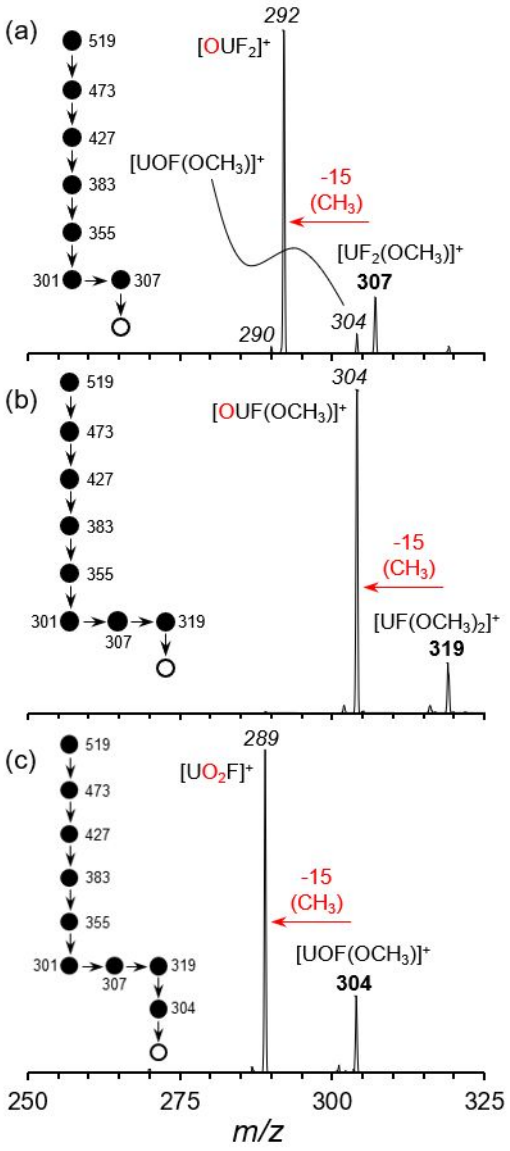

Fig. 3 Product ion spectra generated by CID of ions created by isolating $[UF_2(C_2H)]^+$ for reaction with CH_3OH: (a) CID (MS^9 stage) of $[UF_2(OCH_3)]^+$ at *m/z* 307, (b) CID (MS^9 stage) of $[UF(OCH_3)_2]^+$ at *m/z* 319 and (c) CID (MS^{10} stage) of $[UOF(OCH_3)]^+$ at *m/z* 304. Red font indicates oxo ligands generated by C-O bond cleavage during CID.

longer reactions times (e.g. 100 ms, Figure 2c), additional species such as $[UF(OCH_3)_2]^+$ (*m/z* 319) and $[UF(OCH_3)_2(CH_3OH)]^+$ (*m/z* 351) were observed, and attributed to secondary and tertiary reactions with CH_3OH. To support this suggestion, independent isolation of $[UF_2(OCH_3)]^+$ (*m/z* 307) for reaction with CH_3OH (Figure S2 of the supplemental information) produced $[UF(OCH_3)_2]^+$ and $[UF(OCH_3)_2(CH_3OH)]^+$, most likely by reactions 3 and 4.

(2) $[UF_2(C_2H)]^+ + CH_3OH \rightarrow [UF_2(OCH_3)]^+ + C_2H_2$.
(3) $[UF_2(OCH_3)]^+ + CH_3OH \rightarrow [UF(OCH_3)_2]^+ + HF$
(4) $[UF(OCH_3)_2]^+ + CH_3OH \rightarrow [UF(OCH_3)_2(CH_3OH)]^+$

After creation of $[UF_2(OCH_3)]^+$ at *m/z* 307 by reaction 2, isolation and subsequent CID of the species (MS^9 stage, Figure 3a) caused the elimination of 15 Da to generate a product ion at *m/z* 292. The elimination of 15 Da reflects homolytic cleavage of a methoxide O-C bond, retention of O^{2-} by the U metal center, and ejection of CH_3^+. In any case, we assume that the dissociation reaction leads to oxidation of U formally to the V oxidation state and that the CID reaction results in the creation of $[OUF_2]^+$.

CID (MS^9 stage, Figure 3b) of $[UF(OCH_3)_2]^+$ at *m/z* 319, after its creation from $[UF_2(OCH_3)]^+$ by secondary reaction with CH_3OH, also causes the elimination of 15 Da (assumed again to be CH_3^+) to make $[OUF(OCH_3)]^+$ at *m/z* 304. Subsequent CID (MS^{10} stage, Figure 3c) of $[OUF(OCH_3)]^+$ caused the elimination of 15 Da to create the terminal product ion at *m/z* 289, which was assigned as $[UO_2F]^+$. Therefore, the two sequential CID steps (MS^9 and MS^{10}) initiated with $[UF(OCH_3)_2]^+$ at *m/z* 319 essentially regenerate the two "-yl" oxo ligands through cleavage of O-CH_3 bonds, and reform the UO_2 moiety.

As shown in Figure S3a-c of the supporting information, similar results were obtained using $[UF(OCH_3)_2(CH_3OH)]^+$ at *m/z* 351, created by addition of CH_3OH to $[UF(OCH_3)_2]^+$ (reaction 4). At the MS^8 stage (Figure S3a) CID of $[UF(OCH_3)_2(CH_3OH)]^+$ caused the elimination of 20 Da (HF) to generate $[U(OCH_3)_3]^+$ at *m/z* 331, and the elimination of 32 Da (CH_3OH) to make $[UF(OCH_3)_2]^+$ at *m/z* 319. The elimination of 15 Da (CH_3^+) was observed again in two subsequent stages: CID (MS^9 stage, Figure S3b) of $[U(OCH_3)_3]^+$ at *m/z* 331 created $[UO(OCH_3)_2]^+$ at *m/z* 316, which fragmented (MS^{10} stage, Figure S3c) to leave a terminal product ion at *m/z* 301, which is assigned as $[UO_2(OCH_3)]^+$. CID of the *m/z* 319 derived from fragmentation of $[UF(OCH_3)_2(CH_3OH)]^+$ matched the spectrum shown in Figure 3b, collected by dissociation of the *m/z* 319 ion created instead by reaction of $[UF_2(OCH_3)]^+$ with CH_3OH.

The ion trap modified for ion-molecule reaction studies does not have the high resolution or mass accuracy necessary for the *m/z* measurements that aided composition assignment discussed above for the MS^n CID of $[UO_2(O_2C\text{-}C_6F_2H_3)(CH_3CH_2OH)_2]^+$. Therefore, to support composition assignments in the ion-molecule reaction/CID studies that involved species created in "bottom up" fashion by reaction with CH_3OH, we re-ran the experiments using CD_3OH as the neutral reagent admitted into the ion trap. The data collected for the labeled ions are summarized in scheme S1, and in the spectra provided in Figures S4 and S5 of the supporting information. For the ions generated by reaction(s) of $[UF_2(C_2H)]^+$ with CD_3OH, the neutral losses created by cleavage of O-CD_3 bonds (O-CH_3 for the unlabeled complexes) shifted to 18 Da (CD_3^+). The difference of 3 Da indicates the presence of three H atoms in the neutral losses of 15 Da indicated in Figure 2, and is consistent with elimination of d_3-methyl carbocation, and retention of O^{2-} in the product ion.

The last step was to test the hypothesis that the "bottom up" ion-molecule reaction and CID experiments lead to true uranyl species such as $[UO_2(F)]^+$ and $[UO_2(OCH_3)]^+$. To confirm that the terminal product ion generated by CID of $[UF(OCH_3)_2]^+$ is $[UO_2(F)]^+$, we used a solution of $UO_2(F)_2$ to generate the $[UO_2(F)]^+$ cation (*m/z* 289) directly by electrospray ionization. The species was then isolated and allowed to react with H_2O in

the ion trap for periods ranging from 10 ms to 1 s (Figure S6a-c of the supplemental information). With increased reaction time, the intensity of $[UO_2(F)]^+$ at *m/z* 289 decreased, while the intensity of a product ion at *m/z* 287, assigned as $[UO_2OH]^+$, increased, consistent with (hydrolysis) reaction 5.

As shown in the spectra in Figure S6d-f, the same reactivity was displayed when the ion at *m/z* 289, generated instead in serial CID experiments with $[UF(OCH_3)_2]^+$, was independently isolated and exposed to H_2O. This observation supports our hypothesis that the ion at *m/z* 289 created in the "bottom up" process by CID of $[UF(OCH_3)_2]^+$ is actually $[UO_2(F)]^+$.

In a previous study[11k] we investigated the fragmentation of $[UO_2(OCH_3)]^+$ that was created by MS^n CID of precursors such as $[UO_2(OCH_3)(CH_3OH)_2]^+$ and $[UO_2(NO_3)(CH_3OH)_2]^+$. The $[UO_2(OCH_3)]^+$ ion dissociates for form product ions at *m/z* 270 and 271. The former is created by elimination of methoxy radical, $\bullet OCH_3$, while the latter is generated by rearrangement, H-transfer and elimination of $O{=}CH_2$[11k]. In Figure S7, the product ion spectrum (Figure S7a) generated by CID of $[UO_2(OCH_3)]^+$ derived in MS^n experiments initiated with methanol coordinated uranyl-methoxide cation ($[UO_2(OCH_3)(CH_3OH)_2]^+$) is compared to the spectrum resulting from dissociation of the ion at *m/z* 301 that was created in the "bottom up" experiments in the present study by fragmenting $[UF(OCH_3)_2(CH_3OH)]^+$ (Figure S7b). Both spectra contain the product ion peaks at *m/z* 270 and 271 at similar relative intensities when created by CID under similar experimental conditions. Therefore, the similarity of the fragmentation patterns for both species supports the hypothesis that $[UO_2(OCH_3)]^+$ is generated by CID of $[U(OCH_3)_3]^+$ in the "bottom up" experiments in the present study.

4 Conclusions

To summarize, we have shown here using multiple-stage (MS^n) tandem mass spectrometry experiments that CID of a precursor ion with composition $[UO_2(O_2C\text{-}C_6F_2H_3)(CH_3CH_2OH)_2]^+$ drives the elimination of the CH_3CH_2OH ligands, and decarboxylation, to create what is assumed to be a gas-phase complex that contains UO_2^{2+} and a difluorophenide ligand. Subsequent CID causes elimination of CO, followed by the combined loss of CO and C_2H_2, from $[UO_2(C_6F_2H_3)]^+$ in sequential dissociation steps to leave $[UF_2(C_2H)]^+$. Dissociation of $[UF_2(C_2H)]^+$ creates $[UF_2]^+$ as the terminal product ion, which displays complete substitution of both axial oxo ligands from the initial UO_2^{2+} core. The accurate mass measurement data unambiguously identify neutral losses of small species such as CO and C_2H_2, and confirm the molecular formulae of the product ions created at each CID stage. Because the $[UF_2(C_2H)]^+$ species is generated after the elimination of the CH_3CH_2OH ligands from the precursor complex ion, the elimination of CO signals the decomposition of the UO_2 moiety and what we assume is the pendant 2,6-difluorophenide ligand. The observed loss of 2 CO molecules in the MS^n experiments further supports the hypothesis of axial oxo ligand activation and substitution.

While the mechanism by which $[UF_2(C_2H)]^+$ is created in the MS^n CID sequence is not clear, and remains under investigation, an intriguing hypothesis is that F transfer from 2,6-difluorophenide to UO_2 during CID creates a pendant aryne ligand. Arynes are highly reactive, have electrophilic character and are susceptible to reactions with nucleophiles[13]. In the present case, the nucleophile(s) would be the axial oxo ligands of UO_2. Generation of such a ligand in the condensed phase might provide a novel route for oxo-substitution/elimination.

Our experiments also reveal that the 2,6-difluorophenide complex with UO_2^{2+} is a convenient precursor for highly reactive species that contain U(IV), for which gas-phase data is relatively scarce. Reaction of $[UF_2(C_2H)]^+$ with CH_3OH creates $[UF_2(OCH_3)]^+$ and C_2H_2, and $[UF_2(OCH_3)]^+$ in turn reacts with CH_3OH to furnish $[UF(OCH_3)_2]^+$ and HF, demonstrating the increased lability of the fluoride ligands as compared to the axial oxo ligands. Cleavage of C-O bonds, with elimination of 15 Da, is caused in two subsequent CID steps to convert $[UF(OCH_3)_2]^+$ to $[UO_2(F)]^+$. Similar steps can be used to produce $[UO_2(OCH_3)]^+$ from $[U(OCH_3)_3]^+$. To the best of our knowledge, our experiments represent the first demonstration that both axial oxo ligands can be activated and removed in "top-down" CID reactions, and subsequently regenerated by "bottom-up" ion-molecule and dissociation steps.

Author Contributions

MJV: Conceptualization, Methodology, Writing – original draft, Project administration. EHP: Investigation, Methodology and Validation. LJM: Investigation, Methodology and Validation. ARB: Investigation, Methodology and Validation. TAC: Conceptualization, Methodology, Writing – review & editing. AS: Investigation, Methodology and Validation.

Conflicts of interest

There are no conflicts to declare.

Acknowledgements

M.V.S. and T.A.C. acknowledge support for this work from the Bayer School of Natural and Environmental Sciences (BSNES) and Duquesne University. Laboratory space renovation was made possible with support from the National Science Foundation through grant CHE-0963450. E.H.P. and A.R.B. acknowledge BSNES, Duquesne University and the National Science Foundation (CHE-1659823) for support of their summer undergraduate research. This work was also supported in part by the Robert Dean Loughney Faculty Development Endowment of Duquesne University. High accuracy mass measurements were performed using the resources of the Ohio State University Campus Chemical Instrumentation Center, supported by NIH Grant P30 CA016058.

Notes and references

1 S. Fortier, T. W. Hayton, Oxo ligand functionalization in the uranyl ion (UO_2^{2+}). *Coord. Chem. Rev*. 2010, **254**, 197 – 214.

2 R. J. Baker, New reactivity of the uranyl(VI) ion. *Chem. Eur. J*. 2012, **18**, 16258 – 16271.

3 M. B. Jones, A. J. Gaunt, Recent developments in synthesis and structural chemistry of non-aqueous actinide complexes. *Chem. Rev*. 2013, **113**, 1137 – 1198.

4 B. E. Cowie, J. M. Purkis, J. Austin, J. B. Love, P. L. Arnold, Thermal and photochemical reduction and functionalization chemistry of the uranyl dication, $[U^{VI}O_2]^{2+}$. *Chem. Rev*. 2019, **119**, 10595-10637.

5 P. L. Arnold, J. B. Love, D. Patel, Pentavalent uranyl complexes. *Coord. Chem. Rev*. 2009, 253, 1973-1978.

6 M. J. Sarsfield, M. Helliwell, Extending the chemistry of the uranyl ion: Lewis acid coordination to a U=O oxygen. *J. Am. Chem. Soc*. 2014, **126**, 1036 - 1037.

7 (a) P. Arnold, D. Patel, A. J. Blanke, C. Wilson, J. B. Love, Selective oxo functionalization of the uranyl ion with 3d metal cations. *J. Am. Chem. Soc*. 2006, **128**, 9610 – 9611; (b) P. L. Arnold, D. Patel, C. Wilson, J. B. Love, Reduction and selective oxo group silylation of the uranyl dication. *Nature*, 2008, **451**, 315 – 317.; (c) G. M. Jones, P. L. Arnold, J. B. Love, Controlled deprotection and reorganization of uranyl oxo groups in a binuclear macrocyclic environment. *Angew. Chem. Int. Ed*. 2012, **51**, 12584 – 12587.; (d) N. L. Bell, P. L. Arnold, J. B. Love, Controlling uranyl oxo group interactions to group 14 elements using polypyrrolic Schiff-base macrocyclic ligands, *Dalton Trans.* 2016, **45**, 15902 – 15909.; (e) P. L. Arnold, A.-F. Pecharman, E. Hollis, A. Yahia, L. Maron, A. Parsons, J. B. Love, Uranyl oxo activation and functionalization by metal cation coordination. *Nat. Chem*. 2010, **12**, 1056 – 1061.; (f) P. L. Arnold, E. Hollis, G. S. Nichol, J. B. Love, J.-C. Griveau, R. Caciuffo, N. Magnani, L. Maron, L. Castro, A. Yahia, S. O. Odoh, G. Schreckenback, Oxo-functionalization and reduction of the uranyl ion through lanthanide-element bond hemolysis: synthetic, structural, and bonding analysis of a series of singly reduced uranyl-rare earth 5f1-4fn complexes. *J. Am. Chem. Soc*. 2013, **135**, 3841 – 3854; (g) P. L. Arnold, A.-F. Pecharman, R. M. Lord, G. M.; Jones, E. Hollis, G. S. Nichol, L. Maron, J. Fang, T. Davin, J. B. Love, Control of oxo-group functionalization and reduction of the uranyl ion. *Inorg. Chem*. 2015, **54**, 3702 – 2710.; (h) M. Zegke, G. S. Nichol, P. L. Arnold, J. B. Love, Catalytic one-electron reduction of uranyl(VI) to Group 1 uranyl(v) complexes via Al(III) coordination. *Chem. Commun*., 2015, **51**, 5876-5879. (i) N. L. Bell, B. Shaw, P. L. Arnold, J. B. Love, Uranyl to uranium(IV) conversion through manipulation of axial and equatorial ligands. *J. Am. Chem. Soc*. 2018, **140**, 3378-3384.

8 (a) D. D. Schnaars, G. Wu, T. W. Hayton, Reduction of pentavalent uranyl to U(IV) facilitated by oxo functionalization. *J. Am. Chem. Soc*. 2009, **131**, 17532 – 17533.; (b) T. W. Hayton, G. Wu, Exploring the effects of reduction or Lewis acid coordination on the U=O bond of the uranyl moiety. *Inorg. Chem*. 2009, **48**, 3065 – 3072.; (c) D. D. Schnaars, G. Wu, T. W. Hayton, Silylation of the uranyl ion using $B(C_6F_5)_3$-activated Et_3SiH. *Inorg. Chem*. 2011, **50**, 9642 – 9649; (d) E. A. Pedrick, G. Wu. N. Kaltsoyannis, T. W. Hayton, Reductive silylation of a uranyl dibenzoylmethanate complex: an example of controlled uranyl oxo ligand cleavage. *Chem. Sci*. 2014, **5**, 3204 – 3213.; (e) L. A. Seaman, E. A. Pedrick, G. Wu, T. W. Hayton, Promoting oxo functionalization in the uranyl ion by ligation to ketimides. *J. Organomet. Chem*. 2018, **857**, 34 – 37.; (f) E. A. Pedrick, G. Wu, T. W. Hayton, Oxo ligand substitution in a cationic uranyl complex: synergistic interaction of an electrophile and a reductant. *Inorg. Chem*. 2015, **54**, 7038 – 7044.

9 (a) J. J. Kiernicki, D. P. Cladis, P. E. Fanwick, M. Zeller, S. C. Bart, Synthesis, characterization, and stoichiometric U-O bond scission in uranyl species supported by pyridine(diamine) ligand radicals. *J. Am. Chem. Soc*. 2015, **137**, 11115 – 11125.; (b) E. J. Coughlin, Y. Qiao, E. Lapsheva, M. Zeller, E. J. Schelter, S. C. Bart, Uranyl functionalization mediated by redox-active ligands: generation of O-C- bonds via acylation. *J. Am. Chem. Soc*. 2019, **141**, 1016–1026.

10 A. J. Lewis, P. J. Carroll, E. J. Shelter, Stable uranium(VI) methyl and acetylide complexes and the elucidation of an inverse trans influence ligand series. *J. Am. Chem. Soc*. 2013, **135**, 13185–13192.

11 (a) Y. Gong, V. Vallet, M. Michelini, D. Rios, J. K. Gibson, Activation of gas-phase uranyl: from and oxo to a nitrido complex. *J. Phys. Chem. A*. 2014, **118**, 325 – 330.; (b) Y. Gong, W. A.; de Jong, J. K. Gibson, Gas phase uranyl activation: formation of a uranium nitrosyl complex from uranyl azide. *J. Am. Chem. Soc*. 2015, **137**, 5911 – 5915.; (c) M. J. Van Stipdonk, M. del Carmen Michelini, A. Plaviak, D. Martin, J. K. Gibson, Formation of bare UO_2^{2+} and NUO^+ by fragmentation of gas-phase uranyl-acetonitrile complexes. *J. Phys. Chem. A*. 2014, **118**, 7838 – 7846.; (d) A. Abergel, W. A. de Jong, G. J-P. Deblonde, P. D. Dau, I. Captain, T. M. Eaton, J. Jian, M. J. van Stipdonk, J. Martens, G. Berden, J. Oomens, J. Gibson, Cleaving off uranyl oxygens through chelation: A mechanistic study in the gas phase. *Inorg. Chem*. 2017, **56**, 12930 – 12937; (e) S.-X. Hu, J. Jian, J. Li, J. K. Gibson, Destruction of the uranyl moiety in a U(V) "cation-cation" interaction. *Inorg. Chem*. 2019, **58**, 10148 – 10159.; (f) M. J. van Stipdonk, I. J. Tatosian, A. C. Iacovino, A. R. Bubas, L. Metzler, M. C. Sherman, A. Somogyi, Gas-phase deconstruction of UO_2^{2+}: Mass spectrometry evidence for generation of $[OU^{VI}CH]^+$ by collision-induced dissociation of $[U^{VI}O_2(C{\equiv}CH)]^+$. *J. Am. Soc. Mass Spectrom*. 2019, **30**, 796 – 805; (g) L. J. Metzler, C. T. Farmen, T. A. Corcovilos and M. J. Van Stipdonk. Intrinsic Chemistry of $[OUCH]^+$: Reactions with H_2O, $CH_3C{\equiv}N$ and O_2. *Phys. Chem-Chem. Phys*. 2021, *accepted article*. (h) M. J. Van Stipdonk, I. Tatosian, A. Bubas, E. Perez, N. Polonsky, L. Metzler, A. Somogyi, Formation of $[U^VOF_4]^-$ by Collision-induced Dissociation of a $[U^{VI}O_2(O_2)(O_2C\text{-}CF_3)_2]^-$ Precursor. *Int. J. Mass Spectrom*. 2018, **424**, 58-64.; (i) C. Hanley, W. A. de Jong, M. J. Van Stipdonk, Coming Full Circle: A Computational Density Functional Investigation of Gas-Phase Ions Derived from Uranyl Benzoate and Halogenated Benzoate Precursors, Abstracts, 30th ASMS Sanibel Conference, St. Petersburg, FL, January 25–28, 2018.; (j) C. Hanley, W. A. de Jong, I. Tatosian, L. Metzler and M. Van Stipdonk, An Interdisciplinary Investigation of Uranyl Benzoate or Pentafluorobenzoate Species using Density Functional Theory and High Accuracy Mass Measurements, Proceedings of the 66th ASMS Conference on Mass Spectrometry and Allied Topics, San Diego, CA, June 3-7, 2018.

12 (a) R. A. J. O'Hair, The 3D quadrupole ion trap mass spectrometer as a complete chemical laboratory for fundamental gas-phase studies of metal mediated chemistry. *ChemComm.* 2006, 1469 – 1481. (b) S. Gronert, Estimation of Effective Ion Temperature in a Quadrupole Ion Trap. *J. Am. Soc. Mass Spectrom*. 1998, **9**, 8, 845–848.; (c) W. A. Donald, G. N. Khairallah, R. A. J. O'Hair. The effective temperature of ions stored in a linear quadrupole ion trap mass spectrometer. *J. Am. Soc. Mass Spectrom*. 2013, **24**, 811-815.

13 (a) E. V. Anslyn and D. A. Dougherty, *Modern Physical Organic Chemistry*, University Science Books, 2006, p612.; (b) T. L. Gilchrist, Supplement C: *The Chemistry of Triple Bonded*

Functional Groups, Part 1. Patai, S.; Rappaport, Z. Eds., John Wiley & Sons, New York, 1983 .